

Operator and entanglement growth in non-thermalizing systems: many-body localization and the random singlet phase

Ian MacCormack,^{1,*} Mao Tian Tan,^{1,†} Jonah Kudler-Flam,^{1,‡} and Shinsei Ryu^{1,2,§}

¹*Kadanoff Center for Theoretical Physics,
University of Chicago, Chicago, IL 60637, USA*

²*James Franck Institute, University of Chicago, Chicago, Illinois 60637, USA*

Abstract

We characterize the growth and spreading of operators and entanglement in two paradigmatic non-thermalizing phases — the many-body localized phase and the random singlet phase — using out-of-time-ordered correlators, the entanglement contour, and operator entanglement. We contrast these phases with strongly thermalizing holographic conformal field theories and fully localized Anderson insulators. We obtain a phenomenological description of the operator and state dynamics of these phases and demonstrate the utility of the entanglement contour and operator entanglement measures as useful probes of slowly scrambling and non-thermalizing dynamics.

* imaccormack@uchicago.edu

† mtan1@uchicago.edu

‡ jkudlerflam@uchicago.edu

§ ryuu@uchicago.edu

Contents

I. Introduction	3
A. Summary of Results	5
II. MBL in the Disordered Heisenberg Model	6
A. Global Quench	9
B. Operator Entanglement and Negativity	12
C. Local Quench	13
D. OTOC	15
III. Random Singlet Phase	15
A. Global Quench	17
B. Operator Entanglement and Negativity	20
C. Local Quench Contour Dynamics	21
D. OTOC	22
IV. Discussion	24
V. Conclusion	26
A. Operator Entanglement and Negativity for free fermions	27
1. Operator State for Free Fermions	27
2. Alternate form of Operator State	28
3. Correlator Method	29
B. Correlator method for local operator quench	31
C. Quasi-particle Calculation of Entanglement Entropy after a Global Quench in the RSP	32
D. Anderson Localization Results	33
References	34

I. Introduction

In recent years, the study of chaos and thermalization in out-of-equilibrium quantum systems has received much attention. Generically, interacting quantum systems pushed out of equilibrium with some finite energy density rapidly reach equilibrium and become describable (locally) by a thermal ensemble. This can be understood as a process of information loss, in which the local details of the initial state are spread out, or scrambled, across all degrees of freedom, becoming inaccessible to local measurements [1–3].

While most works on quantum chaos and thermalization have focused on systems that obey the eigenstate thermalization hypothesis (ETH) and rapidly scramble information, a number of recent papers have investigated slowly scrambling systems [4–11], indicating a rich variety of dynamical behavior in systems that do not reach thermal equilibrium, or do so exponentially slowly. In order to better understand this behavior, we will compute a number of entanglement and operator growth measures in three important classes of non-thermalizing systems; the Anderson insulator, the many-body localized (MBL) phase, and the random singlet phase (RSP).

To study entanglement production and spreading, we will use the entanglement contour, which serves as a well-behaved entanglement density function [12]. The entanglement contour has been shown to provide an intuitive picture of the extent to which each degree of freedom in a given subsystem is entangled with the subsystem’s complement. A natural proposal¹ for generic many-body systems is to partition the subsystem, A , into subsets $\{A_i\}$ [14–17]

$$s_A(A_i) = \frac{1}{2} [S(A_i|A_1 \cup \dots \cup A_{i-1}) + S(A_i|A_{i+1} \cup \dots \cup A_n)] \quad (1)$$

where $S(A|B)$ is the conditional entropy

$$S(A|B) \equiv S(A \cup B) - S(B). \quad (2)$$

This gives a quasi-local picture of how entanglement entropy is spreading in a system. For the MBL and RSP phases, it elucidates the nontrivial spatial distribution of entanglement after quantum quenches.

¹ Though not uniquely defined, this definition has been shown to give nearly identical results as other proposals specific to free systems [13].

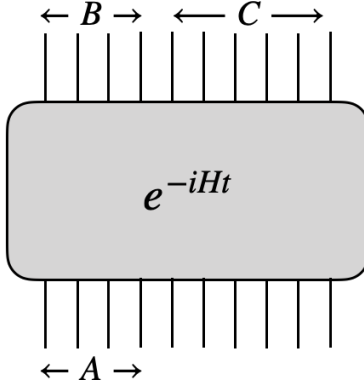


FIG. 1. We show a cartoon of a unitary time evolution operator where both the input and output legs are physical degrees of freedom in the state $H_1 \otimes H_2$. We demonstrate representative partitioning into regions A , B , and C .

Moving from a state to an operator picture, we also compute the out-of-time-ordered correlators (OTOC), specifically $C(t) = \langle \|[V(0,0), W(x,t)]\|^2 \rangle_\beta$, for local operators V and W in all of the aforementioned phases. The OTOC has become a standard measure of operator growth in quantum systems [18–21]. Two local operators that are initially spatially separated will commute (or anticommute in the case of fermions). As the system evolves in time, however, the spatial support of the operators grow, and the operators fail to commute. The OTOC measures this failure i.e. the spatial spreading of the local operators. The speed of the wave front created by the OTOC defines the *butterfly velocity*.

Finally, we compute state-independent measures of information spreading, operator mutual information and negativity. Operationally, this is done by mapping the time evolution operator, $U(t)$, to a state in a doubled Hilbert space, $\mathcal{H}_1 \otimes \mathcal{H}_2$, under channel-state duality [22, 23]. Explicitly, the time evolution operator may be expanded in its energy eigenbasis as

$$U(t) = e^{-iHt} \sum_i |i\rangle \langle i|. \quad (3)$$

We can then dualize the bra vector to define a state in a doubled Hilbert space

$$|U(t)\rangle = \mathcal{N} e^{-iH_1 t} \sum_i |i\rangle_1 |i^*\rangle_2, \quad (4)$$

where we take the CPT conjugate and \mathcal{N} is a normalization factor. The Hamiltonian acts only on the first copy of the Hilbert space. We then compute entanglement measures within this state. Throughout this paper, we let A be a subsystem in the input Hilbert space,

\mathcal{H}_1 , and B, C be subsystems in the output Hilbert space, \mathcal{H}_2 , with $B \cup C = \mathcal{H}_2$ (depicted in Fig. 1). Using these intervals, we can compute bipartite operator mutual information (BOMI) using the standard definition of mutual information [24, 25]

$$I(A, B) = S(A) + S(B) - S(A \cup B), \quad (5)$$

and tripartite operator mutual information (TOMI) by a taking linear combination of BOMIs [26]

$$I_3(A, B, C) = I(A, B) + I(A, C) - I(A, B \cup C). \quad (6)$$

Similarly, we can compute bipartite operator logarithmic negativity (BOLN) simply by computing logarithmic negativity, $\mathcal{E}(A, B) \equiv \log(|\rho_{AB}^{T_B}|_1)$, in the operator state. Analogous to TOMI, we also study the tripartite operator logarithmic negativity (TOLN) introduced in Ref. [27]

$$\mathcal{E}(A; B, C) = \mathcal{E}(A, B) + \mathcal{E}(A, C) - \mathcal{E}(A, B \cup C). \quad (7)$$

The operator entanglement measures allow us to understand the ability of a Hamiltonian to delocalize information, independent of an initial state. TOMI and TOLN, in particular, tell us about the extent to which information in an interval of the input systems becomes delocalized across the output system, and have been proposed as diagnostics of quantum chaos.

A. Summary of Results

Before proceeding to the details of our analysis, we present two tables (Tables I and II) as a convenient summary of our results, as well as previously known results pertaining to the dynamics of disordered systems. The first table contains brief descriptions of quantities related to global quenches: the half-chain von Neumann entropy after a global quench, the entanglement contour after a global quench, and tripartite operator mutual information/negativity. The second table summarizes results related to local operators: the entanglement contour after a local operator quench and out-of-time-ordered correlators. We contrast the free fermion and holographic CFTs, the Random Singlet Phase, the MBL phase, and the Anderson insulator for all quantities. Free fermion and holographic CFTs are included for comparison, as examples of systems that are minimally and maximally scrambling, respectively. Each table contains references to more detailed discussions on each quantity,



FIG. 2. Left: configuration for the global quench with excitations propagating homogeneously throughout the system. Right: configuration for the local operator quench where the single excitation propagates from the origin where the two subintervals meet.

System	$S_A(t)$ after Global Quench	$s_A(x, t)$ after Global Quench	TOMI/TOLN ($t \rightarrow \infty$)
Free Fermion	$\frac{c}{12} \log \left(\frac{\beta}{\pi \epsilon} \sinh \left(\frac{2\pi t}{\beta} \right) \right)$ taking $L \rightarrow \infty$, otherwise, there will be revivals [28]	$\begin{cases} 0 & x < 2t \\ \frac{c\pi}{12\beta} \coth \left(\frac{\pi x}{\beta} \right) = s_A^\beta/2 & x > 2t \end{cases}$ [12, 15, 29]	0 [27, 30]
Holographic CFT	$\frac{c}{12} \log \left(\frac{\beta}{\pi \epsilon} \sinh \left(\frac{2\pi t}{\beta} \right) \right)$ taking $L \rightarrow \infty$, otherwise, there will be revivals [31]	$\begin{cases} 0 & x < 2t \\ \frac{c\pi}{12\beta} \coth \left(\frac{\pi x}{\beta} \right) = s_A^\beta/2 & x > 2t \end{cases}$ [15]	$I_3 = -2S_A$ [30] $\mathcal{E}_3 = -2S_A^{(1/2)}$ [27] These are thermal entropies and are of the largest magnitude possible.
RSP	Complicated quasi-power law growth at early times (Fig. 7), $\log(\log(t))$ at very late times [32]	Power law light cone, $x_c \sim t^\alpha$, with $\alpha \sim 0.264$. $\sim 1/x$ decaying profile at long times (Fig. 8)	Saturation to non-maximal negative value, with no length dependence (Fig. 9). Magnitude decreases as disorder increases.
MBL	$\sim \log t$ (saturation to sub-thermal volume law in finite systems) [33, 34]	Logarithmic light cone, exponentially decaying profile at long times (Fig. 3)	Saturation to negative values (not maximal) at exponentially long times (Fig. 4)
Anderson Localization	Rapid saturation to area law [34]	No entanglement growth/spreading (Fig. 13)	~ 0 (Fig. 14)

TABLE I. Table of global entanglement measures.

either in this work or in other papers. Collectively, the various quantities provide a picture of a diverse range of entanglement and operator growth behavior.

II. MBL in the Disordered Heisenberg Model

Many-body localization (MBL) is perhaps the best known example of ergodicity-breaking in many-body quantum systems. It occurs in interacting systems when an on-site potential is tuned to be sufficiently spatially disordered. MBL has been a subject of intense study in recent years. See, for example, the recent review Ref. [38] and references within. As the strength of the on-site disorder is increased relative to the interaction strength, more and more of the system's high energy eigenstates turn from typical volume law entanglement

System	$s_A(x, t)$ after local operator quench	OTOC $C(t)$
Free CFT	Ballistic propagating wave packet moving at the speed of light [12]	ballistic propagating wave packet. Decay to zero once wave packet passes (i.e. no scrambling) [35, 36]
Holographic CFT	Ballistic propagating wave packet moving at the speed of light $s_A(x) = \begin{cases} \frac{c}{12} \frac{(2x-t)}{x(x-t)} & 0 < t < x \\ \frac{c}{6} \log \left[\frac{\sin(\pi a_\psi)}{\delta \alpha_\psi} \right] \delta(x-t) & t = x \\ \frac{c}{6x} + \frac{c}{12} \frac{1}{t-x} & x < t \end{cases} .$ where $a_\psi = \sqrt{1 - \frac{24h}{c}}$ with h the conformal dimension of the primary operator [15].	Exponential growth (with Lyapunov exponent $\lambda_L = 2\pi/L$) once within the light cone of the operator, regardless of the operator. Scrambling time of $t_* = \frac{\beta}{2\pi} \log c$ and late-time exponential decay as $\propto e^{-2\pi\Delta t/\beta}$ where Δ is the dimension of the operator [19–21].
RSP	Rapid saturation to exponentially decaying profile (Fig. 11)	Very small values for the σ_z, σ_z OTOC away from localized bump at origin, indicating little to no operator spreading. The behavior is essentially identical to that of the Anderson localized case. (Fig. 12)
MBL	Rapid saturation to an exponentially decaying profile. Smaller entanglement growth for quenches with local operators with considerable overlap with the LIOMs (Fig. 5)	Clear operator spreading and saturation along a logarithmic light cone (Refs. [6, 10, 11, 37] and Fig. 6)
Anderson Localization	No spreading (Fig. 13)	Behavior is similar to that of the Random Singlet Phase. (Fig. 12)

TABLE II. Table of local operator measures.

(as the eigenstate thermalization hypothesis would suggest), to short-range entangled area law states [39]. Once the localization transition is passed, all eigenstates of the system become area law entangled, and the system is fully many-body localized. Before reaching the transition, it is possible to have a mobility edge, separating area law from volume law states. In addition to the area law eigenstates, MBL systems display a number of interesting features. In the localized phase, the systems contain an extensive number of emergent local integrals of motion (LIOMs, sometimes called “l-bits”), with exponentially decaying spatial support. One can write an effective Hamiltonian for the MBL system in terms of these LIOMs [40].

MBL systems are also fascinating from a dynamical perspective because they fail to thermalize under unitary time evolution due to the presence of the emergent LIOMs and the resulting area law excited states. Generic interacting many-body quantum systems are thought to be ergodic, and after sufficiently long time evolution — even from a trivial

product state — expectation values of local operators become equal to their corresponding thermal expectation values in a Gibbs ensemble. Thus, memory of the initial state becomes inaccessible to local measurements, and any subsystem can be described by a small number of thermodynamic quantities. MBL systems, on the other hand, do not appear to thermalize after long time evolution by their Hamiltonians (at least in one and two dimensions) [38]. The conserved LIOMs serve to retain memory of the initial state, precluding a description of the late-time state by a thermal ensemble. Since the lack of ergodicity in MBL is closely tied to the short-ranged entangled structure of the high energy eigenstates, MBL provides an important counterexample to the eigenstate thermalization hypothesis (ETH) and motivates us to further understand when and how closed quantum systems fail to thermalize. Furthermore, MBL has been realized in a number of experimental settings [41–43], where its non-ergodic properties have been directly observed, making the system an important starting point for understanding ETH-violating behavior.

Despite their lack of energy and particle transport, MBL systems nevertheless produce nontrivial long range entanglement in far-from-equilibrium scenarios. For example, if we quench into an MBL Hamiltonian starting from a product state, the system will display a (disorder averaged) logarithmic growth of subsystem entanglement entropy [34]. This non-trivial entanglement growth suggests that it may be worthwhile to study the entanglement and operator dynamics in the MBL phase more deeply.

We find the entanglement contour after a global quench to show the emergence of a logarithmic light cone similar to the one seen for the OTOC in previous works. Next, we compute tripartite operator entanglement measures — proposed probes of quantum chaos — yielding a particularly interesting result indicating that while MBL systems do not thermalize, they do scramble information, albeit very slowly.

For direct comparison with much of the recent literature, we will investigate the MBL phase of the disordered Heisenberg model with the following Hamiltonian

$$H = J \sum_i (\sigma_i^x \sigma_{i+1}^x + \sigma_i^y \sigma_{i+1}^y + \sigma_i^z \sigma_{i+1}^z) + \sum_i h_i \sigma_i^z, \quad (8)$$

where h_i is a random variable from the uniform distribution $[-h, h]$. This model is believed to be fully many-body localized for $J = 1$ and $h \gtrsim 7$. As in Ref. [10], we will use $h = 16$ throughout to ensure a short localization length.

A. Global Quench

We perform a global quench from a random product state on 11 sites and average over 400 disorder realizations. That is, in each disorder realization, we construct a random product state in the spin- z basis, time evolve the state with (8), compute the entanglement entropies and contour at each time step, and then average the results for each realization.

The entanglement entropy dynamics after a global quench in MBL is well known (see e.g. Ref. [34]). The entanglement entropy will grow logarithmically for a time that scales exponentially with the system size. After this time, the saturated entanglement entropy in finite systems displays a volume law, though with a smaller multiplicative coefficient than the volume law for the thermal state [44]. In some sense, this volume law indicates a partial thermalization of finite size MBL systems [39].

We study the entanglement contour in order to identify how much entanglement entropy each site in a particular interval is responsible for after the global quench described above. Before appealing to numerics, we motivate an analytical prediction for the form of the entanglement contour in MBL.

The effective interaction between two “l-bits” separated by a distance d is given by [3]

$$J^{eff} \sim J_0 \exp(-d/\xi), \quad (9)$$

where J_0 is the bare interaction (in our case, $J_0 = J_{zz} = 1$) and ξ is the localization length. Using the effective interaction of the dressed spins, one can obtain an estimate for the amount of time it takes for two unentangled l-bits to become entangled. This happens when $J^{eff}t \geq 1$, so

$$t \sim \frac{1}{J_0} \exp(-d/\xi). \quad (10)$$

We now consider an MBL system on a chain of total length L , with a subinterval $[0, \ell]$. Picking a point $x < \ell$ within this subinterval, we can count the number of l-bits outside of the interval with which the l-bit at point x is entangled at a particular time t . This is precisely what the entanglement contour should describe. The result (up to proportionality

constants) is

$$s_\ell(x, t) \propto \begin{cases} 0 & t < \frac{e^{-\frac{\ell-x}{\xi}}}{J_0} \\ \frac{1}{L}(\xi \log(J_0 t) + x - \ell) & \frac{e^{-\frac{\ell-x}{\xi}}}{J_0} \leq t \leq \frac{e^{-\frac{L-x}{\xi}}}{J_0} \\ 1 - \frac{\ell}{L} & t > \frac{e^{-\frac{L-x}{\xi}}}{J_0} \end{cases} \quad (11)$$

The form of the logarithmic light cone is clear; the wave front of the contour arrives at a time $t = \frac{1}{J_0} \exp\left(\frac{\ell-x}{\xi}\right) \rightarrow \ell-x = \xi \log(J_0 t)$. Once this time has passed, the magnitude of the contour increases linearly, saturating at a constant value. This agrees with the observation that entanglement entropy grows logarithmically in MBL, eventually reaching a volume law in the long time limit, as found in [34]. Let us now turn to numerics in order to verify Eq. (11) and to determine the other features of the entanglement contour.

We select a subinterval consisting of the leftmost six sites of our eleven site chain and compute the entanglement contour of this interval after the global quench. We observe a distinct logarithmic light cone in the entanglement contour in Fig. 3. A similar logarithmic light cone has previously been observed in out-of-time-order correlators (OTOCs) of certain local operators in the same disordered Heisenberg model [6, 10, 11, 37]. These are, however, different light cones.

The light cone carved out by the contour indicates which sites have bipartite entanglement with the subsystem's complement, while the OTOC light cone indicates the spatial support of a particular operator in the Heisenberg picture. These can (and generally do) spread at different speeds. Previous works (e.g. [45]) have compared the butterfly velocity with the entanglement velocity², but here we compare the former with the contour velocity, which is the speed of the wave front of the entanglement contour. In 1+1D CFTs with ballistically spreading operator support, one finds that although both the entanglement contour and the OTOC both yield linear light cones, the contour light cone has a velocity that is twice the butterfly velocity, $v_C = 2v_B$. Operator spreading adheres to the Lieb-Robinson bound

² The entanglement velocity characterizes the (non-local) speed at which the entanglement entropy grows and should not be considered physical velocity like the contour and butterfly velocities.

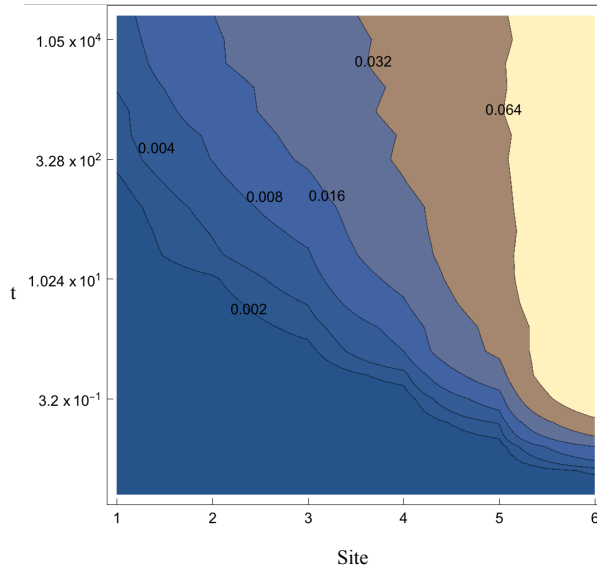


FIG. 3. Entanglement contour after a global quench in the disordered Heisenberg model (averaged over 400 disorder realizations and normalized by $\log 2$, the maximum possible onsite entropy). The horizontal axis is the site number (with the entanglement cut at the right) and the vertical axis is logarithmic time. The quench was performed from random product states on 11 sites using a disorder strength of $h = 16$. The contour depicted describes the six leftmost sites. Some smoothing of the numerical data was used to more clearly display the level sets of the entanglement contour.

[46, 47], while entanglement spreading does not³. We should thus expect that the contour velocity after a global quench in MBL to be greater than the butterfly velocity in the same system, though not necessarily by a full factor of two.

In Ref. [10], the authors computed the OTOC as a function of space and time in the disordered Heisenberg model. They do so for several operators both in an eigenstate as well as for thermal states at various temperatures. Defining the butterfly “velocity,” v_B , as

$$j \sim v_B \log_{10} t, \quad (12)$$

where j is the site at which the wave front of the OTOC exists at time t (in units of inverse coupling constant, using a particular cutoff value, $\epsilon \in (0, 1)$), they find that v_B depends on both temperature and ϵ , with a slower speed of propagation for lower temperatures. Though we are limited by our small system size, we can make an attempt at computing a contour

³ Even so, it is reasonable to consider twice the Lieb-Robinson velocity as a bound on the contour velocity.

velocity — at least within an order of magnitude — for the MBL global quench. We can define the contour velocity analogously as

$$j_c \sim v_c^\epsilon \log_{10} t \quad (13)$$

where j_c is the site that the contour wave front of value $\epsilon \times s_A^\beta$ has reached. Looking at the smallest possible discernible wave front in Fig. 3, we can choose $\epsilon \times s_A^\beta = 0.002$. Using this cutoff, and fitting a line to the wave front in Fig. 3, we arrive at a contour velocity of $v_c^\epsilon \sim 2$. This is based on the observation that our selected wave front takes approximately 2×10^2 units of time to traverse five sites. Of course, this result is highly dependent on our choice of cutoff ϵ , and may also depend on our choice of initial state. The point remains, however, that entanglement spreading after a global quench in MBL as measured by the entanglement contour, occurs much more quickly than the spreading of operators as measured by the OTOC in Ref. [10] and reproduced in Fig. 6, where $v_B \sim 1$. More sophisticated numerical study (perhaps using tensor network methods) of the entanglement contour after a global quench in MBL is warranted [48–53]. This would allow simulation on much larger system sizes, taking advantage of the emergent integrability of MBL systems. Performing simulations for larger system sizes using various initial states should yield a more precise understanding of the relationship between v_B and v_c in MBL. We leave this for future work.

B. Operator Entanglement and Negativity

In MBL systems, operator entanglement was first studied in Ref. [54]. We would like to extend this work by computing the tripartite operator mutual information and logarithmic negativity which should provide a clear window into the information scrambling capabilities of MBL Hamiltonians.

We find slow scrambling in the tripartite operator mutual information and tripartite operator logarithmic negativity as seen in Fig. 4. While a significant portion of the information in the input channel is delocalized under time evolution, the Haar random values of TOMI and TOLN are never reached⁴. Intriguingly, it appears that the scrambled *quantum information* (TOLN) may scale differently with system size than the *total information* (TOMI).

⁴ See Ref. [55] for discussion on more quantum systems that scramble non-maximally.

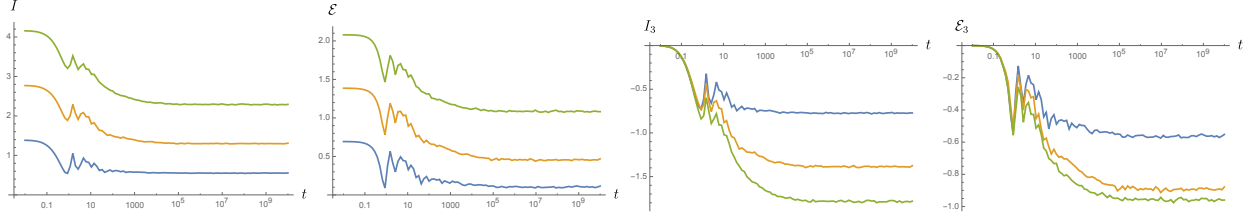


FIG. 4. Operator entanglement measures for MBL. The spin chain has six input and six output spins. The BOMI and BOLN (left) are for symmetric intervals at one end of the chain of lengths 1, 2, and 3 sites. The TOMI and TOLN (right) are for the same intervals. The results are averaged over 100 disorder realizations. Note the logarithmic time scale, indicating slow scrambling.

By “total,” we are referring to both the quantum and classical (thermal) correlations to which mutual information is sensitive (see e.g. Ref. [56]). Since negativity probes purely quantum correlations, the larger magnitude of the tripartite mutual information for MBL points to possible *spurious entanglement*, meaning the TOMI may mislead us to think that the system has scrambled more quantum information than it truly has. Our system sizes, however, are limited by exact diagonalization to 6 sites (12 sites in the doubled Hilbert space).

Regardless of the finite-size limitations, the saturation of the operator entanglement measures at nontrivial values points to some sort of quasi-thermalization, as does the finite size saturation seen in the entanglement entropy. It would be very interesting to distinguish this late-time state from conventional scrambled states.

C. Local Quench

While the global quench and operator entanglement analyses reveal the novel aspects of entanglement growth and thermalization in MBL, further analysis is needed to understand the propagation of local operators. In local operator quenches, we start in the ground state of the Hamiltonian and insert a local operator — either σ_i^x , σ_i^z , or $\sigma_i^x + \sigma_i^z$ — driving the system out of equilibrium. The entanglement contour then tracks how the information of this local operator insertion spreads across the system in time.

We choose the same six site interval as before and insert the local operator at site six at $t = 0$. The resulting entanglement contours for the operators σ_6^x , $\frac{1}{\sqrt{2}}(\sigma_6^x + \sigma_6^z)$, and

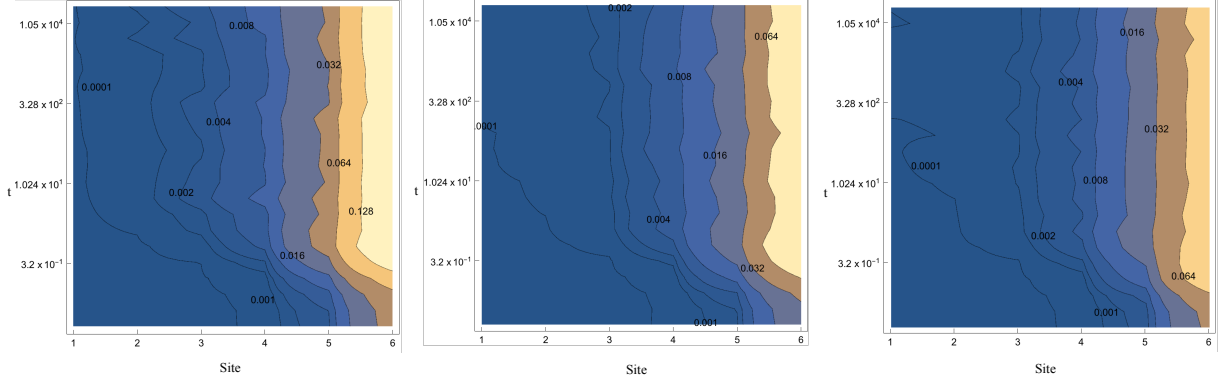


FIG. 5. Left: Entanglement contour after local quench with σ_6^x . The horizontal axis is the site number (with the entanglement cut at the right) and the vertical axis is logarithmic time. Center: The contour after a local quench with $\frac{1}{\sqrt{2}}(\sigma_6^x + \sigma_6^z)$. This operator has partial overlap with the LIOMs. Right: The entanglement contour in the case of the σ_6^z local quench. This operator has a large overlap with the LIOMs. None of the operator quenches resulted in significant entanglement spreading. All plots were averaged over 100 disorder realizations and normalized by $\log 2$.

σ_6^z can be seen in Fig. 5. In all three of the operator quenches, it is difficult to discern any clear entanglement spreading from the entanglement contour. Soon after the initial operator insertion, the contour equilibrates to what appears to be an exponentially decaying profile i.e. the entanglement growth ceases. This makes sense intuitively because all of the eigenstates of an MBL system can be expressed as product states of the l-bits. When we act, for example, with σ_6^x , a single l-bit is flipped, bringing the state close to another product state of l-bit configurations (another eigenstate).

The small amount of entanglement spreading we do see may be attributed to the quasi-local nature of the l-bits. The l-bit at a particular site has a nonzero but exponentially decaying overlap with physical spins near that site. Thus, when we act on a physical spin at one site, we are also slightly perturbing l-bits at nearby sites. These perturbations rapidly die off in time, resulting in the equilibration to a state with a single flipped l-bit. While Refs. [6, 10, 11, 37] demonstrated nontrivial spreading of certain operators in MBL via the OTOC, it appears that the same operators do not produce significant entanglement in a local quench procedure. The entanglement contour captures this process in a fairly intuitive picture, confirming our intuition about dynamics in MBL.

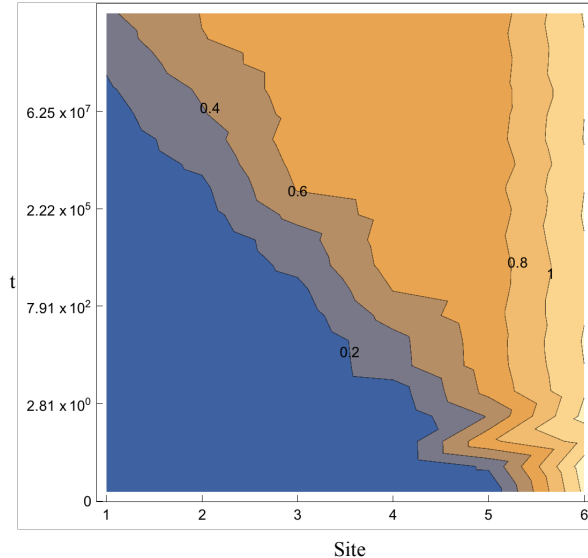


FIG. 6. OTOC of σ_6^x and $\sigma_j^x(t)$ for the disordered Heisenberg model on six sites, averaged over 100 disorder realizations. The logarithmic light cone is clearly visible.

D. OTOC

To complete our analysis of slow scrambling in MBL systems, we compute the expectation value of the commutator squared. For MBL systems, the linear light cone is replaced by a logarithmic one, as shown in Refs. [4, 5, 10, 11]. We reproduce this logarithmic light cone in Fig. 6. The contour velocity in Fig. 3 is larger than the butterfly velocity of the OTOC which is to be expected because the OTOC has only one operator evolving in time while the global quench has all operators evolving in time. A zeroth order approximation then has $v_c \simeq 2v_B$. This is exactly true for 2D CFTs, but only a rough approximation generally.

III. Random Singlet Phase

In this section, we study the dynamics of a disordered free fermion model (described in Ref. [57]) that exhibits a transition between a topological and a trivial Anderson localized phase. At the critical point, the model exhibits a random singlet phase [58, 59]. The RSP critical point has a number of interesting features, including CFT-like logarithmic scaling of entanglement entropy in the ground state [60, 61], with an effective central charge equal

to $\log 2$ times the central charge of the clean theory. The RSP is the fixed point of the strong disorder real space renormalization group (SDRG), and can also be seen in e.g. the antiferromagnetic random bond Heisenberg model [62]. It should be noted, however, that the universal features of the RSP ground state seen at the SDRG fixed point do not extend to excited states in interacting models. Indeed, while the RSP-like critical behavior extends to the excited states of a noninteracting model like the one we use here (resulting in a so-called “quantum critical glass” [63, 64]), small interactions can drive these excited states to a MBL spin glass phase. Studying the dynamics of an interacting model with a RSP ground state using the entanglement measures in this paper presents an interesting future problem. Some work in this direction has recently been done [65], and it is found that the resulting particle-hole symmetric MBL phase exhibits entanglement growth behavior whose functional form depends on interaction strength, unlike conventional MBL.

Additional work has been done to investigate the dynamics of the random singlet phase. For example, Ref. [32] studied the late time growth of entanglement entropy in the RSP after a global quench using numerical methods and found it to be doubly logarithmic in time. Other works have studied entanglement growth in disordered critical phases e.g. Refs. [66, 67]. We build upon this work and calculate additional quantities that should give us further insight into the dynamics of the RSP.

We will use a free fermion model with a topological phase transition that can be shown to be equivalent to the RSP via a Jordan-Wigner transformation. The model and its phase diagram are outlined in Ref. [57]. The Hamiltonian is

$$H = \sum_i \left[\frac{t_i}{2} \left(c_i^\dagger (\sigma_1 + i\sigma_2) c_{i+1} + h.c. \right) + m_i c_i^\dagger \sigma_2 c_i \right], \quad (14)$$

where c_i and c_i^\dagger are two component fermions and the hopping and onsite potentials are

$$t_i = 1 + \omega_i \Delta J, \quad m_i = m + \omega'_i \Delta m. \quad (15)$$

Here, $\omega_i, \omega'_i \in [-0.5, 0.5]$ are two independent random variables that simulate disorder, while ΔJ and Δm control the strength of the disorder. For the clean case, we have $\Delta J = \Delta m = 0$. We can tune m to get the topological SSH ground state for $m < 1$ and a trivial gapped ground state for $m > 1$. At exactly $m = 1$, we have a $c = 1$ critical point. When we add disorder by using nonzero values of ΔJ and Δm , we change the location of the phase transition as a function of m . The new critical point is the random singlet phase, with

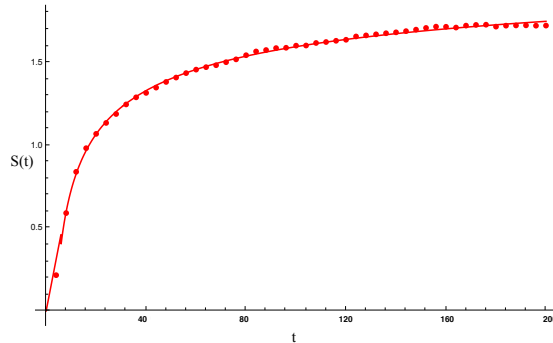


FIG. 7. Half chain entanglement entropy growth after a global quench into the random singlet phase for a system of 100 sites. After an initial linear increase, the entropy grows approximately as a power law before transitioning to a sub-logarithmic regime. The numerical results (dots) are averaged over 3000 disorder realizations. The analytic estimate for the entanglement entropy is displayed as a solid line. We fit using $\beta_{eff} = 1.06$. The analytic estimates derived from the quasi-particle picture show excellent agreement with the numerics.

effective central charge $c = \log 2$. For example, setting $\Delta J = 1$ and $\Delta m = 2$, the critical point appears to occur around $m = 1.1$. In the disordered system, the topological phase becomes a localized topological phase, and the trivial gapped state becomes an Anderson insulator.

A. Global Quench

The quench into the random singlet phase provides another example of intermediate dynamics between full localization and full thermalization. The initial state is the half-filled ground state of (14) with the following parameters: $t = 1.0, m = 1.8, \Delta J = 0, \Delta m = 0$. This ensures that we are well inside of the gapped, disorderless phase where correlation lengths are short, so that entanglement is short-ranged. At time $t = 0$, we quench to the random singlet phase by instantaneously changing the parameters to $t = 1.0, m = 1.1, \Delta J = 1, \Delta m = 2$.

The entanglement entropy growth is depicted in Fig. 7. Qualitatively, we see an initial linear growth, followed by what appears to be a power law growth, which eventually settles to a very slow, sub-logarithmic growth. In order to obtain an analytical estimate for the

entanglement dynamics, we have used the quasi-particle picture. Since we are using a free fermion model, the quasi-particle picture is applicable. The master formula is [68]

$$S(t) \propto t \int_{|v(E)|t < \ell} dE v(E) f(E) + \ell \int_{|v(E)|t > \ell} dE f(E), \quad (16)$$

where ℓ is the length of the interval, $v(E)$ is the velocity of the quasi-particles at energy E and $f(E)$ is the entanglement production rate of quasi-particles. In other words, $f(E)$ is the extent to which each mode contributes to the entanglement entropy. For this function, we can use the entropy of each occupied fermionic mode

$$f(E) = S(n(E)) = -(1 - n(E)) \log(1 - n(E)) - n(E) \log n(E), \quad (17)$$

where $n(E)$ is the occupation number of each mode after the quench. The Fermi-Dirac distribution provides an excellent approximation for this

$$n(E) = \frac{1}{1 + e^{\beta_{eff} E}}. \quad (18)$$

Here, β_{eff} is an effective inverse temperature, determined by the energy of the initial, pre-quench state.

Using the density of states for the infinite disorder RG fixed point, we can compute the velocity of the associated quasi-particles [69]

$$\rho(E) = \frac{\rho_0}{E |\log E|^3} \quad \rightarrow \quad v(E) = \frac{E |\log E|^3}{\rho_0}. \quad (19)$$

The above density of states is quite unusual, though we have verified it numerically, reassuring us that we are closely approximating the infinite disorder fixed point. It displays a concentration of low energy “slow” modes between $E = 0$ and $E = 1$. These may be responsible for the long-time growth of entanglement entropy. It should be emphasized, however, that the above density of states comes from the fixed point of a real space RG procedure, and is only expected to be valid asymptotically as $E \rightarrow 0$. Using the standard form for the semiclassical particle velocity, $v(E) = \left. \frac{dE(k)}{dk} \right|_{k(E)}$, which we have done, is also not exactly correct, since the eigenstates of the disordered model are not labeled by momentum k . Disorder averaging, however, restores approximate translational symmetry, and the above form of the quasi-particle velocities yields results consistent with numerics. The remaining details of this calculation can be found in Appendix C. The analytical form of the entanglement

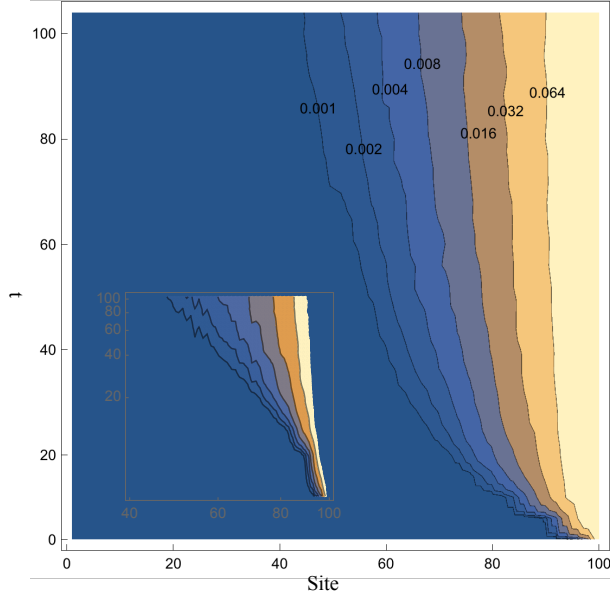


FIG. 8. Entanglement contour for the leftmost 100 sites in an open chain of size 200, averaged over 500 disorder realizations and normalized by $\log 2$. The parameters used for this simulation were $\Delta J = 1.0$, $\Delta m = 2.0$, and $m = 1.1$. We see the emergence of a power-law light cone for the entanglement contour, approximately following $x_c \sim t^\alpha$, with $\alpha \sim 0.264$. If we tune m below or above this critical point, we observe a completely localized entanglement contour profile in the topological and Anderson phases, respectively (see Appendix D). The inset show the same data on a log-log scale to make the power-law light cone manifest.

entropy is very complicated and not terribly enlightening, but appears to agree well with the numerical results in the plot shown in Fig. 7.

We will now use the contour to investigate finer grained aspects of the entanglement entropy growth. The result of a global quench from a gapped ground state at half filling can be seen in Fig. 8. Though the production of entanglement is weaker than it is in the clean limit, the contour certainly demonstrates nontrivial spreading, and carves out a novel power-law light cone. Picking the $s(x, t) = 0.001$ contour from Fig. 8, we see that the wave front of the contour approximately follows the curve $x_c \sim t^\alpha$, with $\alpha \sim 0.264$.

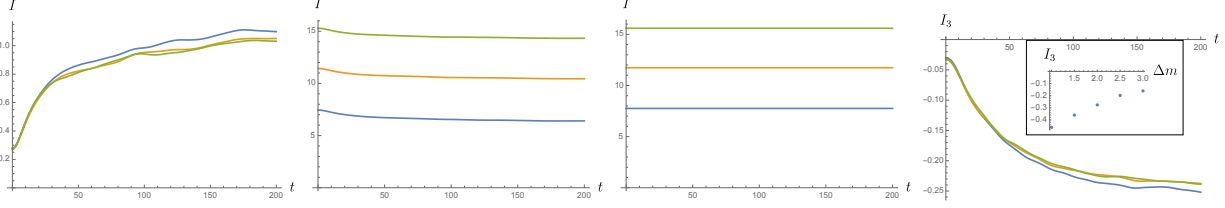


FIG. 9. The top left, top right and bottom graphs correspond to I_{AB} , I_{AC} , $I_{A,BC}$ and $I_3(A, B, C)$ in the Random Singlet phase, respectively, where the subsystems are $A = [X_2, X_1]$, $B = [Y_2, Y_1]$ and $C = [Y_4, Y_3]$. The total number of sites is 200, and the inverse temperature of the corresponding TFD state is $\beta = 2\epsilon = 20$. The blue, yellow and green curves correspond to $X_1 = Y_3 = 50, 75, 100$ respectively, where $X_2 = Y_4 = 1$ and subsystem B is taken to be the complement of C . In other words, $Y_2 = Y_3 + 1$ and $Y_1 = L$. The quantities are averaged over 400 disorder realizations. The parameters are chosen to be $m = 1.1, \Delta J = 1, \Delta m = 2$.

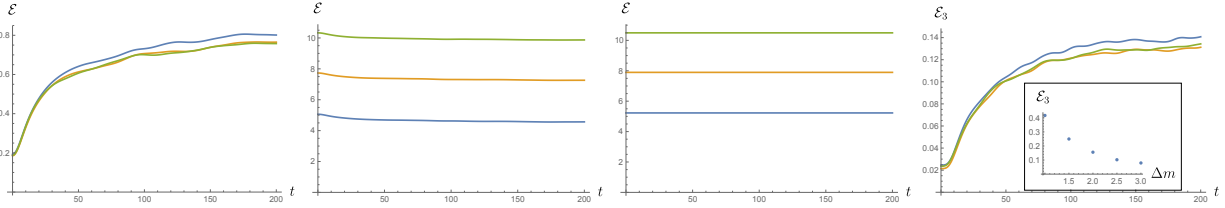


FIG. 10. The top left, top right and bottom graphs correspond to \mathcal{E}_{AB} , \mathcal{E}_{AC} , $\mathcal{E}_{A,BC}$ and $\mathcal{E}_3(A, B, C)$ in the Random Singlet phase, respectively, where the subsystems are $A = [X_2, X_1]$, $B = [Y_2, Y_1]$ and $C = [Y_4, Y_3]$. The total number of sites is 200, and the inverse temperature of the corresponding TFD state is $\beta = 2\epsilon = 20$. The blue, yellow and green curves correspond to $X_1 = Y_3 = 50, 75, 100$ respectively, where $X_2 = Y_4 = 1$ and subsystem B is taken to be the complement of C . The quantities are averaged over 400 disorder realizations. The parameters are chosen to be $m = 1.1, \Delta J = 1, \Delta m = 2$.

B. Operator Entanglement and Negativity

We now compute operator entanglement measures in the random singlet phase. The results are shown in Fig. 9. The BOMI is consistent with the quasi-particle picture with a non-trivial dispersion relation. In the graph for I_{AB} , we see that some quasi-particles from subregion A enter subregion C , causing an increase in I_{AC} . On the other hand, some of the quasi-particles leave subregion B , which has been chosen to have the same spatial support as

subregion A , causing a slight decrease in I_{AB} . Note that $I_{A,BC}$ is time independent. This is because the unitary operator state is a pure state and the complement of $A \cup BC$ is a spatial region located only on the first Hilbert space, so $S_{A,BC}$ is time-independent. The tripartite mutual information is negative and appears to saturate at some value that is independent of the subsystem size. Naively, we would then be led to believe that there is some amount of scrambling. However, we will see that this nontrivial I_3 is actually a finite size effect, which disappears as we go deeper into the RSP. In the inset of Fig. 9, we show a plot of $I_3(t = 200)$ as we vary the disorder strengths ΔJ and Δm with their ratios fixed. The parameters $m, \Delta J, \Delta m$ have to be tuned to remain in the random singlet phase. A plot of $\mathcal{E}_3(t = 200)$ against Δm is shown in the inset of Fig. 10. The ratio between ΔJ and Δm is kept fixed, and m is adjusted so as to remain in the random singlet phase. The magnitudes of both tripartite operator mutual information and tripartite operator logarithmic negativity decrease as disorder strength is increased. This indicates that the “scrambling” we observe in the RSP vanishes as we move deeper into the phase, and the nontrivial values of I_3 and \mathcal{E}_3 we observed are merely a result of finite size.

C. Local Quench Contour Dynamics

We perform a local quench in the RSP by initializing our system in the half-filled ground state of our model (using the same parameters as in the global quench), and applying the following local operator

$$\hat{\sigma}_j^z = 2\hat{c}_j^\dagger \hat{c}_j - 1, \quad (20)$$

at the site $j = L/2$. We then time evolve with the RSP Hamiltonian, computing the entanglement contour at each time step, and averaging the result over disorder realizations.

The resulting entanglement contour can be seen in Fig. 11. At early times, we see diffusive spreading of entanglement along a linear light cone, which soon dies off, leaving a steady state entanglement contour. There is considerably more entanglement spreading than in the Anderson case, which points to some amount of weak operator spreading. Investigating the OTOC of the same local operator will allow us to understand this weak scrambling more clearly.

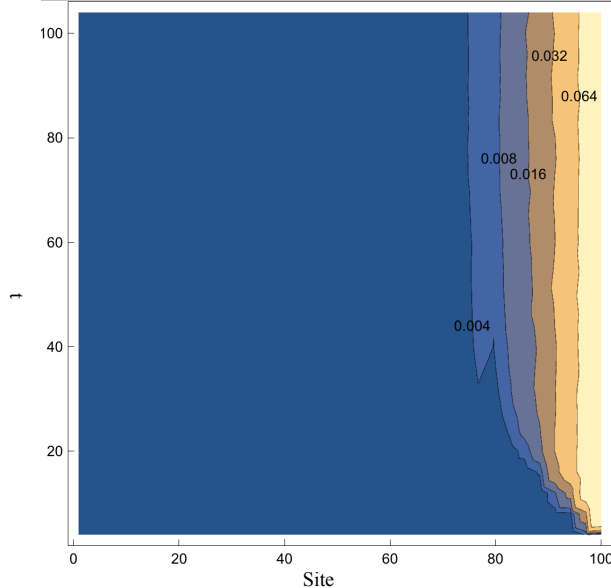


FIG. 11. The entanglement contour for the left half of our chain after a local quench with σ^z at site $L/2$ in the RSP. The parameters used are $m = 1.1$, $\Delta J = 1.0$ and $\Delta m = 2.0$ and the numerics were done on a lattice of 200 sites. We see some short range spreading of entanglement entropy, which soon dies out and results in a contour similar to that of the RSP ground state, albeit with a slightly larger magnitude. The results for the contour were averaged over 500 disorder realizations, normalized by $\log 2$, and the ground state entanglement contour was subtracted off to provide a clearer picture of entanglement spreading.

D. OTOC

We also compute OTOCs with the same operator, to closely compare the operator spreading with the entanglement spreading induced by the same local operator. The results indicate that although the local quench produces a small, but nonzero amount of entanglement spreading, there is negligible operator spreading. This is similar to the Anderson localized system, in which case there is no spreading of either the operator support or the entanglement contour. We have included results from the Anderson insulator in Appendix D for direct comparison with the random singlet phase.

In this section, we show the result for an OTOC in the RSP. Using the Jordan-Wigner transformation, we can turn the fermionic model into a spin-1/2 model, making the compu-

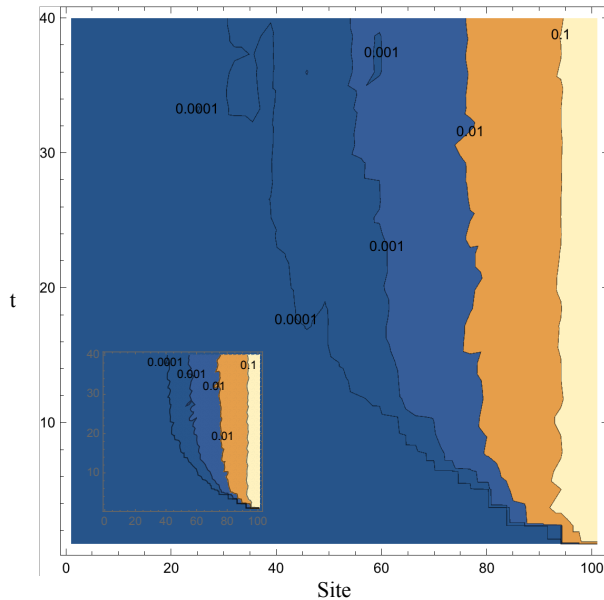


FIG. 12. Plot of commutator squared $C(x, t)$ for the 100 sites to the left of σ_i^z in the random singlet phase. The parameters are set to $m = 1.1, \Delta J = 1, \Delta m = 2$. The results are averaged over 400 disorder realizations. (inset) The same quantity computed in the Anderson localized phase. The two plots are virtually identical, indicating that the random singlet phase displays essentially no operator spreading, at least for σ^z .

tation slightly easier. We compute the following correlator:

$$C(x, t) = \langle [\hat{\sigma}_i^z(t), \hat{\sigma}_j^z]^\dagger [\hat{\sigma}_i^z(t), \hat{\sigma}_j^z] \rangle \quad (21)$$

where i, j label sites in the spin model and $x = i - j$.

A plot of C as a function in both space and time is shown in Fig. 12. This particular OTOC does not seem to distinguish between the random singlet phase and the Anderson localized phase. Computing the OTOC for some other pairs of operators yields similar results. It is interesting that although the RSP seems capable of producing a nontrivial amount of entanglement entropy, the OTOC does not reveal much about operator spreading. This further justifies the use of a wide array of measures for understanding the dynamics of the RSP and other non-thermalizing systems.

IV. Discussion

Contour velocity vs. butterfly velocity

In this paper, we have considered two distinct, but related, velocities; the contour velocity and the butterfly velocity. Following a global quantum quench, the entanglement contour propagates from the entangling surfaces. The contour velocity is the speed at which the wave front propagates. One must impose some cutoff value of the contour in order to define the wave front. On the other hand, the butterfly velocity corresponds to the speed at which local operators spread, in contrast to the contour velocity which corresponds to the speed at which correlations spread. The butterfly velocity is defined through the out-of-time-ordered correlator (OTOC). Naturally, the contour velocity and butterfly velocity will be related. They are, in general, different speeds partially because the OTOC only time evolves one of the operators in the correlation function, while the entanglement contour probes time evolved *states* i.e. all operators are time evolved. Because all operators have been given the chance to spread in time, the contour velocity will be roughly twice as fast as the butterfly velocity. In 2d conformal field theories, it is true that $v_c = 2v_B$, and it appears to be approximately true (in logarithmic time) in MBL. It would be interesting to check the relationship between v_c and v_B in higher dimensions where the relationship between the butterfly and entanglement velocity non-trivial.

Late-time quasi-Equilibration of MBL

Though we are working with very small system sizes, we see that the saturated TOMI and TOLN values do not scale linearly with subsystem size in MBL, which they do in ergodic channels [27, 30]. They are, however, nontrivially negative, whereas they saturate to zero for free homogeneous systems and Anderson localized systems. This, combined with the slow spreading of the contour and the logarithmic growth of entanglement, indicates that although MBL does not transport particles or energy, it is capable of spreading some quantum information over long periods of time. The late time saturation of subsystem entanglement entropy to a volume law and of TOMI leads us to wonder about the nature of this late-time state. It is clearly not fully thermalized, since it still retains memory of the initial LIOMs, yet it displays volume law entanglement, and the MBL time evolution operator clearly causes some amount of slow scrambling. Is this a different sort of “thermalized” quasi-equilibrium state? Can it be characterized by a sort of generalized Gibbs ensemble?

Generic scrambled pure states are described by so-called canonical thermal pure quantum (cTPQ) states [70], which describe all of the late time thermal behavior of local operators in thermalizing systems. Perhaps a generalization of such states could describe the late-time, partially scrambled state after a global quench in MBL.

Lack of Eigenstate Thermalization

An implication of the eigenstate thermalization hypothesis (ETH) is that generic excited states of nonintegrable many-body systems demonstrate volume law subsystem entanglement entropy, assuming the subsystem is sufficiently small. Although most forms of ETH require nonintegrability, the volume law entanglement can be seen in many integrable systems as well. The excited eigenstates of our Hamiltonian (14) tuned to the random singlet phase, in contrast, do not display volume law entanglement, instead showing logarithmic growth — like its ground state. This sub-volume law entanglement is at the root of the slow dynamics we see in the RSP.

Although we use a free fermionic model for the RSP, the phase is also realized as the ground state of interacting models with disordered hopping, in particular the spin- $\frac{1}{2}$ antiferromagnetic Heisenberg chain [71]. Further investigation of dynamics in an interacting model exhibiting a RSP ground state is an interesting avenue for future work.

Decoupling of Entanglement and Operator Spreading

The difference in the butterfly velocity and the contour velocity (after a global quench) already highlights the essential difference in the phenomena of operator spreading and of entanglement spreading. The difference in behavior between the OTOC and the entanglement contour after a local quench in the RSP provides another example of this difference. Although both quantities ostensibly probe the consequences of perturbing the system with the same operator — in our case σ_i^z — they yield very different information. The OTOC tells us that there is little to no spreading of the support of the initially local σ_i^z operator. On the other hand, if we perform a local quench using σ_i^z acting on the ground state, then compute the entanglement contour, we see that the operator causes small but nontrivial entanglement spreading. It is thus crucial to analyze a variety of both operator and state measures when trying to understand the information spreading properties of a particular system. One may miss interesting aspects of the dynamics of the RSP and other systems by focusing solely on the OTOC or the entanglement entropy. The precise relations between the operator and state information measures used in this paper is something that warrants

further study.

V. Conclusion

In summary, we have investigated the non-equilibrium dynamics of two distinct non-thermalizing phases; many-body localization, and (a free fermion realization of) the random singlet phase. Calculating the entanglement contour after a global quench revealed a logarithmic light cone of entanglement spreading in MBL. This light cone was similar, but not identical to the logarithmic light cone seen for the OTOC. Meanwhile, in the RSP, the entanglement contour yielded a novel power-law light cone, despite trivial spreading of the OTOC in that system. Moving on, we calculated operator mutual information and negativity for both of these systems. We found that, unlike the Anderson insulator, the many-body localized system demonstrated slow, but nontrivial saturation of tripartite operator mutual information and negativity, to values smaller in magnitude than in the Haar-random case. This indicates a level of weakly-scrambled quasi equilibration in MBL, which warrants further investigation with more sophisticated numerical methods. The RSP, on the other hand, demonstrated tripartite operator measures that decayed to zero with increasing disorder, indicating that they were a finite size effect, and that, despite its nontrivial entanglement spreading, the RSP does not delocalize quantum information. All together, these results indicate a broad range of behavior of state and operator dynamics between clean, free particle systems and the maximally scrambling holographic or Haar-random systems. Other systems worth investigating include models with quasiperiodic potentials [6], Floquet systems [72], and random unitary circuits with measurements [73].

As entanglement measures become more experimentally accessible, the ubiquity of disorder in physical systems could make slowly scrambling systems an interesting testbed for quantum information dynamics in the lab. Many-body localization has been realized experimentally in several different settings, including superconducting qubits [74] and cold atom systems [75]. Information theoretic measures, in particular the quantum Fisher information [41] and the second Rényi entanglement entropy [43, 76], have become tractable in the lab. As experiments continue to improve, it would be interesting to see other entanglement measures measured experimentally in MBL and other disordered systems.

Acknowledgments

We thank Dmitry Abanin, Masahiro Nozaki, Hassan Shapourian, and Masaki Tezuka for useful comments. SR is supported by a Simons Investigator Grant from the Simons Foundation.

A. Operator Entanglement and Negativity for free fermions

In this appendix, we present a review of how to compute operator entanglement measures for free fermions using the correlator method.

1. Operator State for Free Fermions

We wish to compute the operator mutual information for the following state

$$|U_\beta(t)\rangle = e^{-\frac{it}{2}(\hat{H}_A + \hat{H}_B)} |TFD_\beta\rangle \quad (\text{A1})$$

for a free fermion Hamiltonian with no superconducting terms

$$\hat{H} = \sum_{i,j=1}^L H_{i,j} c_i^\dagger c_j \quad (\text{A2})$$

where we impose open boundary conditions. We can diagonalize it with unitary matrices U , so $H = UDU^\dagger$.

$$\hat{H} = \underbrace{c_i^\dagger U_{ik}}_{\psi_k^\dagger} D_{kl} \underbrace{U_{lj}^\dagger c_j}_{\equiv \psi_l} = \psi_k^\dagger D_{kl} \psi_l = \epsilon_k \psi_k^\dagger \psi_k \quad (\text{A3})$$

We can write down the thermofield double state with the fermions in the diagonal basis.

$$\begin{aligned} |TFD_\beta\rangle &= \frac{1}{\sqrt{Z}} \prod_k \left(\sum_{i_k} e^{-\frac{\beta}{2} \epsilon_k \psi_k^\dagger \psi_k} |i_k\rangle |i_k\rangle \right) \\ &= \frac{1}{\sqrt{Z}} \prod_k \left(|0\rangle_k + e^{-\frac{\beta}{2} \epsilon_k} \hat{\psi}_{Ak}^\dagger \hat{\psi}_{Bk}^\dagger |0\rangle_k \right) \\ &= \frac{1}{\sqrt{Z}} \prod_k \left(1 + e^{-\frac{\beta}{2} \epsilon_k} \hat{\psi}_{Ak}^\dagger \hat{\psi}_{Bk}^\dagger \right) |0\rangle \end{aligned} \quad (\text{A4})$$

The state is required to be normalized.

$$\begin{aligned}
1 &= \langle TFD_\beta | TFD_\beta \rangle \\
Z &= \langle 0 | \prod_k \left(1 + e^{-\frac{\beta}{2}\epsilon_k} \hat{\psi}_{Bk} \hat{\psi}_{Ak} \right) \prod_q \left(1 + e^{-\frac{\beta}{2}\epsilon_q} \hat{\psi}_{Aq}^\dagger \hat{\psi}_{Bq}^\dagger \right) | 0 \rangle \\
&= \prod_k \langle 0 | \left(1 + e^{-\frac{\beta}{2}\epsilon_k} \hat{\psi}_{Bk} \hat{\psi}_{Ak} \right) \left(1 + e^{-\frac{\beta}{2}\epsilon_q} \hat{\psi}_{Ak}^\dagger \hat{\psi}_{Bk}^\dagger \right) | 0 \rangle \\
&= \prod_k \langle 0 | \left(1 + e^{-\beta\epsilon_k} \hat{\psi}_{Bk} \hat{\psi}_{Ak} \hat{\psi}_{Ak}^\dagger \hat{\psi}_{Bk}^\dagger \right) | 0 \rangle \\
&= \prod_k (1 + e^{-\beta\epsilon_k})
\end{aligned} \tag{A5}$$

The normalized thermofield double state is

$$\begin{aligned}
|TFD\rangle &= \prod_k \left(\frac{1}{\sqrt{1 + e^{-\beta\epsilon_k}}} + \frac{e^{-\frac{\beta}{2}\epsilon_k}}{\sqrt{1 + e^{-\beta\epsilon_k}}} \hat{\psi}_{Ak}^\dagger \hat{\psi}_{Bk}^\dagger \right) | 0 \rangle \\
&= \prod_k \left(\underbrace{\frac{e^{\frac{\beta}{2}\epsilon_k}}{\sqrt{1 + e^{\beta\epsilon_k}}}}_{\equiv \cos \theta_k} + \underbrace{\frac{1}{\sqrt{1 + e^{\beta\epsilon_k}}}}_{\equiv \sin \theta_k} \hat{\psi}_{Ak}^\dagger \hat{\psi}_{Bk}^\dagger \right) | 0 \rangle
\end{aligned} \tag{A6}$$

The time evolved state becomes

$$\begin{aligned}
|U(t)\rangle &= e^{-\frac{it}{2}(\hat{H}_A + \hat{H}_B)} |TFD_\beta\rangle \\
&= \prod_k \left(\cos \theta_k + \sin \theta_k e^{-it\epsilon_k} \hat{\psi}_{Ak}^\dagger \hat{\psi}_{Bk}^\dagger \right) | 0 \rangle
\end{aligned} \tag{A7}$$

2. Alternate form of Operator State

In this subsection, we will rewrite the operator state (A7) by using the holes of the B Hilbert space instead of the particles because this allows us to use the regular correlation matrix without pairing terms. Let χ_{Ak} , χ_{Bk} be new fermion operators and consider

$$\begin{aligned}
&\prod_k \left(\cos \theta_k \chi_{Bk}^\dagger + \sin \theta_k e^{-it\epsilon_k} \chi_{Ak}^\dagger \right) | 0 \rangle_\chi \\
&= \prod_k \left(\cos \theta_k + \sin \theta_k e^{-it\epsilon_k} \chi_{Ak}^\dagger \chi_{Bk} \right) \prod_q \chi_{Bq}^\dagger | 0 \rangle_\chi.
\end{aligned} \tag{A8}$$

Define $\chi_{Ak} = \psi_{Ak}$, $\chi_{Bk} = \psi_{Bk}^\dagger$ and note that $| 0 \rangle_\psi \sim \prod_q \chi_{Bq}^\dagger | 0 \rangle_\chi$ because $\psi_{Bp} | 0 \rangle_\psi \sim \chi_{Bp}^\dagger \prod_q \chi_{Bq}^\dagger | 0 \rangle_\chi = 0$ since $(\chi^\dagger)^2 = 0$. The ψ and χ fermions are related by a particle-hole

transformation on H_B . Next, we show that the state is already normalized

$${}_{\chi} \langle 0 | \prod_q (\cos \theta_q \chi_{Bq} + \sin \theta_q e^{it\epsilon_q} \chi_{Aq}) \prod_k (\cos \theta_k \chi_{Bk}^\dagger + \sin \theta_k e^{-it\epsilon_k} \chi_{Ak}^\dagger) | 0 \rangle_{\chi}. \quad (\text{A9})$$

Note that the two momentum products are in reversed order relative to each other. Also, for each momentum, we have a product of the following two factors

$$\begin{aligned} & (\cos \theta_p \chi_{Bp} + \sin \theta_p e^{it\epsilon_p} \chi_{Ap}) (\cos \theta_p \chi_{Bp}^\dagger + \sin \theta_p e^{-it\epsilon_p} \chi_{Ap}^\dagger) \\ &= \cos^2 \theta_p \chi_{Bp} \chi_{Bp}^\dagger + \sin^2 \theta_p \chi_{Ap} \chi_{Ap}^\dagger + \dots \\ &= 1 + \dots \end{aligned} \quad (\text{A10})$$

where $+\dots$ stand for the terms that will annihilate the vacuum. Next, we wish to compute the correlators for this state written in terms of the χ_{Ik} fermions.

$$|U(t)\rangle = \prod_k (\cos \theta_k \chi_{Bk}^\dagger + \sin \theta_k e^{-it\epsilon_k} \chi_{Ak}^\dagger) |0\rangle \quad (\text{A11})$$

where it is understood that $|0\rangle = |0\rangle_{\chi}$.

3. Correlator Method

Now we compute the correlation matrix

$$\langle U(t) | \chi_{Ik}^\dagger \chi_{Jk'} | U(t) \rangle \quad (\text{A12})$$

Note that if $k \neq k'$, $\chi_{Ik}^\dagger \chi_{Jk'} = -\chi_{Jk'} \chi_{Ik}^\dagger$ will annihilate $|U(t)\rangle$ because

$$\langle \dots (\cos \theta_k \chi_{Bk} + \sin \theta_k e^{it\epsilon_k} \chi_{Ak}) \chi_{Ik}^\dagger (\cos \theta_k \chi_{Bk}^\dagger + \sin \theta_k e^{-it\epsilon_k} \chi_{Ak}^\dagger) \dots \rangle = 0 \quad (\text{A13})$$

This leads to the simplification

$$\langle U(t) | \chi_{Ik}^\dagger \chi_{Jk'} | U(t) \rangle = \delta_{kk'} \langle U(t) | \chi_{Ik}^\dagger \chi_{Jk} | U(t) \rangle \quad (\text{A14})$$

Suppose that the product over momenta in (A11) is arranged in increasing order. The matrix element for each momentum k is

$$\begin{aligned} \langle U(t) | \chi_{Ik}^\dagger \chi_{Jk} | U(t) \rangle &= \langle 0 | \prod_{q>k} (\cos \theta_q \chi_{Bq} + \sin \theta_q e^{it\epsilon_q} \chi_{Aq}) \times \\ &\quad \left[(\cos \theta_k \chi_{Bk} + \sin \theta_k e^{it\epsilon_k} \chi_{Ak}) \chi_{Ik}^\dagger \chi_{Jk} (\cos \theta_k \chi_{Bk}^\dagger + \sin \theta_k e^{-it\epsilon_k} \chi_{Ak}^\dagger) \right] \\ &\quad \prod_{p>k} (\cos \theta_p \chi_{Bp}^\dagger + \sin \theta_p e^{-it\epsilon_p} \chi_{Ap}^\dagger) | 0 \rangle \end{aligned} \quad (\text{A15})$$

Let us compute the term in the square bracket for the four possible values of (I, J) . We drop all terms that go to zero when inserted in the correlator.

$I = A, J = A:$

$$\sin \theta_k e^{it\epsilon_k} \chi_{Ak} \chi_{Ak}^\dagger \chi_{Ak} \sin \theta_k e^{-it\epsilon_k} \chi_{Ak}^\dagger = \sin^2 \theta_k \quad (\text{A16})$$

$I = A, J = B:$

$$\sin \theta_k e^{it\epsilon_k} \chi_{Ak} \chi_{Ak}^\dagger \chi_{Bk} \cos \theta_k \chi_{Bk}^\dagger = \sin \theta_k \cos \theta_k e^{it\epsilon_k} \quad (\text{A17})$$

$I = B, J = A:$

$$\cos \theta_k \chi_{Bk} \chi_{Bk}^\dagger \chi_{Ak} \sin \theta_k e^{-it\epsilon_k} \chi_{Ak}^\dagger = \sin \theta_k \cos \theta_k e^{-it\epsilon_k} \quad (\text{A18})$$

$I = B, J = B:$

$$\cos \theta_k \chi_{Bk} \chi_{Bk}^\dagger \chi_{Bk} \cos \theta_k \chi_{Bk}^\dagger = \cos^2 \theta_k \quad (\text{A19})$$

The correlators are

$$\langle U(t) | \chi_{Ik}^\dagger \chi_{Jk'} | U(t) \rangle = \delta_{kk'} \begin{pmatrix} \sin^2 \theta_k & \sin \theta_k \cos \theta_k e^{it\epsilon_k} \\ \sin \theta_k \cos \theta_k e^{-it\epsilon_k} & \cos^2 \theta_k \end{pmatrix}$$

To compute entanglement entropy, we need to the correlation matrix in real space. For a general position space Hamiltonian,

$$\begin{aligned} \hat{H} &= \sum_{x,y} \chi_x^\dagger H_{xy} \chi_y \\ &= \sum_{x,y} \underbrace{\chi_x^\dagger V_{xk}}_{\chi_k^\dagger} \underbrace{D_{kq}}_{\epsilon_k \delta_{kq}} \underbrace{V_{qy}^\dagger}_{\chi_q} \chi_y \\ &= \sum_k \epsilon_k \chi_k^\dagger \chi_k \end{aligned} \quad (\text{A20})$$

the correlation matrix is

$$\begin{aligned} C(x, x', I, J) &= \langle U(t) | \chi_{Ix}^\dagger \chi_{Jx'} | U(t) \rangle \\ &= \sum_{kk'} V_{kx}^\dagger V_{x'k'} \langle U(t) | \chi_{Ik}^\dagger \chi_{Jk'} | U(t) \rangle \\ &= \sum_k V_{kx}^\dagger V_{x'k} \begin{pmatrix} \sin^2 \theta_k & \sin \theta_k \cos \theta_k e^{it\epsilon_k} \\ \sin \theta_k \cos \theta_k e^{-it\epsilon_k} & \cos^2 \theta_k \end{pmatrix} \\ &= \sum_k V_{xk}^* \begin{pmatrix} \sin^2 \theta_k & \sin \theta_k \cos \theta_k e^{it\epsilon_k} \\ \sin \theta_k \cos \theta_k e^{-it\epsilon_k} & \cos^2 \theta_k \end{pmatrix} V_{kx'}^t \end{aligned} \quad (\text{A21})$$

The von Neumann entropy is then given by

$$S(t) = - \sum_k [\xi_k(t) \ln \xi_k(t) + (1 - \xi_k(t)) \ln(1 - \xi_k(t))] \quad (\text{A22})$$

where $\xi_k(t)$ are the eigenvalues. For the truncated correlation matrix where we only keep the entries corresponding to degrees of freedom in our subsystem.

B. Correlator method for local operator quench

In this appendix, we explain how to use the correlator method to efficiently compute entanglement entropy and logarithmic negativity following a local operator quench. We follow Appendix A of Ref. [13] in describing global quantum quenches. We then use a trick to apply the global quench technique to local operator quenches.

We consider N fermions on a lattice and seek to construct the correlation matrix $C_{rr'} \equiv \langle \psi_r^\dagger \psi_{r'} \rangle$. Because we are concerned with quantum quenches, we must specify our two free fermionic Hamiltonians which may be diagonalized as

$$H_0 = \sum_{n=1}^N \tilde{\epsilon}_n g_n^\dagger g_n, \quad H_1 = \sum_{n=1}^N \epsilon_n f_n^\dagger f_n. \quad (\text{B1})$$

These are related to the original fermion operators by unitary transforms

$$g_n^\dagger = \sum_r \varphi_n(r) \psi_r^\dagger, \quad f_n^\dagger = \sum_r \phi_n(r) \psi_r^\dagger, \quad f_n^\dagger = \sum_m U_{nm} g_m^\dagger. \quad (\text{B2})$$

Let us assume that we have started in initial state

$$|\Psi_0\rangle = \prod_{n \in \text{occ.}} g_n^\dagger |0\rangle, \quad (\text{B3})$$

then we may compute the time dependence of the correlation matrix by

$$C_{rr'}(t) = \sum_{n, n'} e^{i(\epsilon_n - \epsilon_{n'})} \phi_n^*(r) \phi_{n'}(r') \sum_{m \in \text{occ.}} U_{nm} U_{n'm}^*. \quad (\text{B4})$$

To apply this formalism to local operator quenches, we diagonalize our Hamiltonian of interest and prepare the ground state (at half-filling)

$$|\Psi\rangle_{gs} = \prod_{n=1}^{N/2} f_n^\dagger |0\rangle. \quad (\text{B5})$$

We then apply our local operator \mathcal{O} to set the (appropriately normalized) initial state

$$|\Psi_0\rangle = \prod_{n=1}^{N/2} \sqrt{\mathcal{N}_n} \mathcal{O} f_n^\dagger |0\rangle. \quad (\text{B6})$$

In order to keep using the correlator method, this operator must keep the state Gaussian. In this work, we have used $\mathcal{O} = (-1)^F$ which is both unitary and Gaussian. Then we simply follow the above procedure for the global quench with

$$g_n^\dagger \equiv \sqrt{\mathcal{N}_n} \mathcal{O} f_n^\dagger. \quad (\text{B7})$$

C. Quasi-particle Calculation of Entanglement Entropy after a Global Quench in the RSP

Combining all of the ingredients mentioned in Eqs. (16-19), we obtain the following integral

$$S(t) \propto \frac{t}{\rho_0} \int_{|v(E)|t < \ell} dE E |\log E|^3 \left(\log(1 + e^{\beta E}) - \frac{\beta E e^{\beta E}}{1 + e^{\beta E}} \right) + \ell \int_{|v(E)|t > \ell} dE \left(\log(1 + e^{\beta E}) - \frac{\beta E e^{\beta E}}{1 + e^{\beta E}} \right). \quad (\text{C1})$$

We can expand the first term to second order in β to get

$$\frac{t}{\rho_0} \int_{|v(E)|t < \ell} dE E |\log E|^3 \left(\log 2 - \frac{E^2 \beta^2}{8} + \mathcal{O}(\beta^4) \right), \quad (\text{C2})$$

which is something we can integrate. In order to get the integration bounds, we must solve

$$v(E)t = \frac{E |\log E|^3 t}{\rho_0} = \ell \quad (\text{C3})$$

for $E > 0$. Since $v(E)$ doesn't increase monotonically with E , there are multiple branches to the solution. In increasing order, they are

$$\exp \left[3W_{-1} \left(\frac{-1}{3} \sqrt[3]{\frac{\ell}{t}} \right) \right], \quad \exp \left[3W \left(\frac{-1}{3} \sqrt[3]{\frac{\ell}{t}} \right) \right], \quad \exp \left[3W \left(\frac{1}{3} \sqrt[3]{\frac{\ell}{t}} \right) \right], \quad (\text{C4})$$

where $W_k(x)$ is the k^{th} branch of the product log or Lambert W-function, and $W(x)$ is the principal branch of the product log function. The first two solutions are only valid (real)

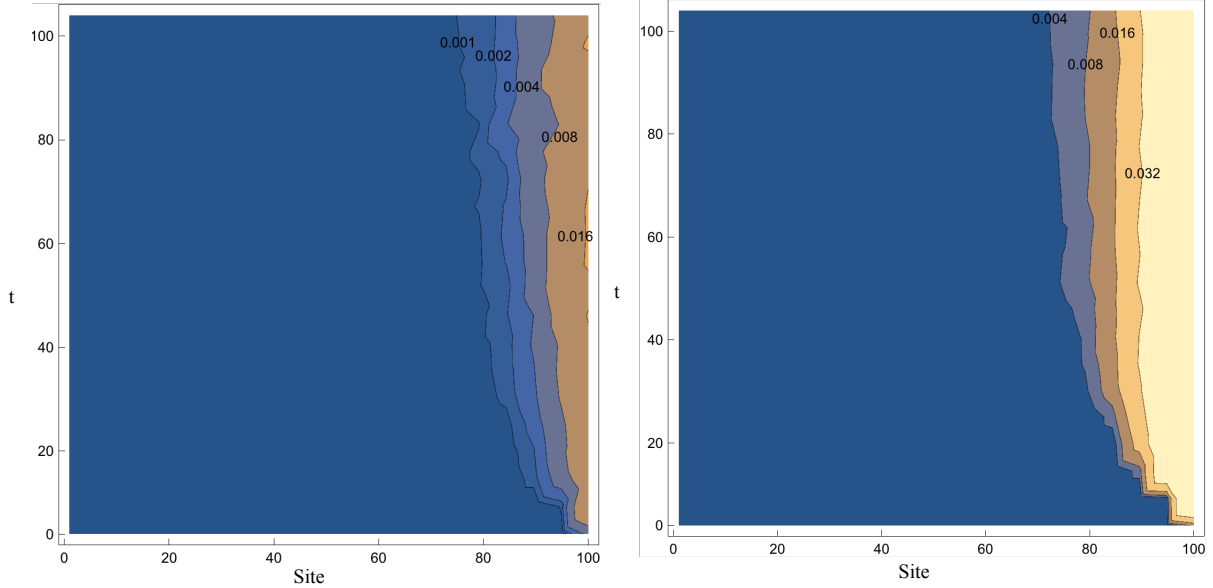


FIG. 13. Left: The entanglement contour after a global quench in the Anderson localized phase. The results are averaged over 100 disorder realizations and normalized by $\log 2$. Essentially no entanglement spreading is evident, as we would expect. Right: Similarly, very little entanglement spreading occurs after a local operator quench in the Anderson localized phase.

for $t > t^* = \frac{e^3 \ell}{27}$, while the third is valid for all $t > 0$. Thus, t^* is the time at which the slow modes begin to contribute to the entanglement growth. This set of slow modes makes the dynamics of the RSP markedly different than that of free fermions.

We can integrate the second term in (C1) without expanding in β . Taking into account once again the multiple domains of integration, and adding an energy cutoff ϵ (which also functions as a velocity cutoff), we obtain a very complicated and unenlightening result for the entanglement entropy, which we have used to fit the numerical data in Fig. 7.

D. Anderson Localization Results

In this appendix, we present numerical results for the entanglement contour and operator entanglement for the Anderson localized system. The results confirm the expectation that the Anderson system displays little to no entanglement and operator spreading.

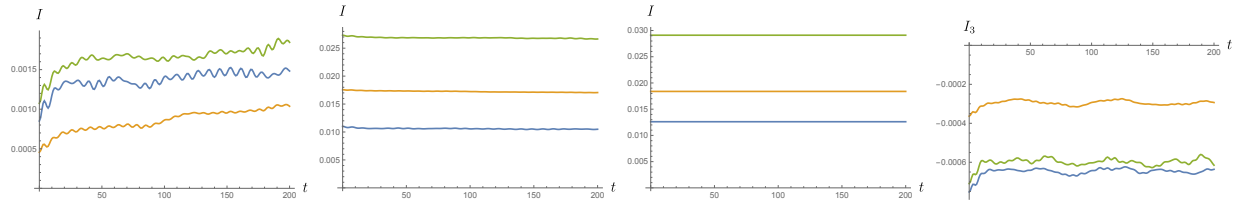


FIG. 14. Plot of bipartite and tripartite operator mutual information against time. From left to right, we have $I_{AB}, I_{AC}, I_{A,BC}$ and $I_3(A, B, C)$ in the Anderson phase. The total number of sites is 200, and the temperature of the corresponding TFD state is $\beta = 2\epsilon = 20$. The blue, yellow and green curves correspond to $X_1 = Y_3 = 50, 75, 100$ respectively, where $X_2 = Y_4 = 1$ and subsystem B is taken to be the complement of C . The quantities are averaged over 20 disorder realizations. The parameters are $m = 1.6, \Delta J = 0.5, \Delta m = 1$.

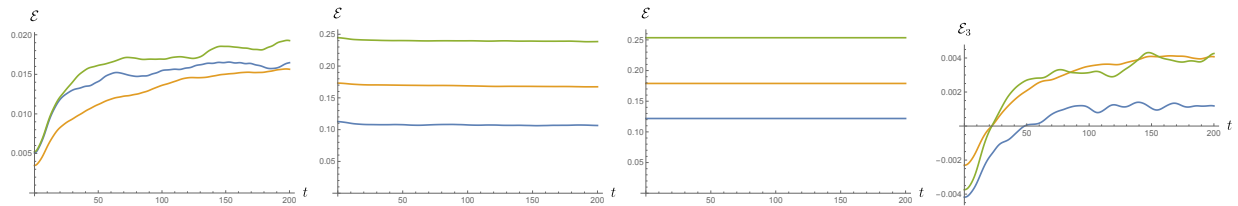


FIG. 15. Plot of bipartite and tripartite operator negativity in the Anderson localizing phase. From left to right, we have $\mathcal{E}_{AB}, \mathcal{E}_{AC}, \mathcal{E}_{A,BC}$ and $\mathcal{E}_3(A, B, C)$. The total number of sites is 200, and the temperature of the corresponding TFD state is $\beta = 2\epsilon = 20$. The blue, yellow and green curves correspond to $X_1 = Y_3 = 50, 75, 100$ respectively, where $X_2 = Y_4 = 1$ and subsystem B is taken to be the complement of C . The quantities are averaged over 20 disorder realizations. The parameters are $m = 1.6, \Delta J = 0.5, \Delta m = 1$.

-
- [1] J.M. Deutsch, *Quantum statistical mechanics in a closed system*, *Phys. Rev. A* **43** (Feb, 1991) 2046.
- [2] M. Srednicki, *Chaos and quantum thermalization*, *Phys. Rev. E* **50** (Aug, 1994) 888 [[cond-mat/9403051](https://arxiv.org/abs/cond-mat/9403051)].
- [3] R. Nandkishore and D.A. Huse, *Many-Body Localization and Thermalization in Quantum Statistical Mechanics*, *Annual Review of Condensed Matter Physics* **6** (Mar, 2015) 15 [[arXiv:1404.0686](https://arxiv.org/abs/1404.0686)].

- [4] Y. Chen, *Universal Logarithmic Scrambling in Many Body Localization*, *arXiv e-prints* (Aug, 2016) arXiv:1608.02765 [[arXiv:1608.02765](#)].
- [5] B. Swingle and D. Chowdhury, *Slow scrambling in disordered quantum systems*, *Phys. Rev. B* **95** (Feb, 2017) 060201 [[arXiv:1608.03280](#)].
- [6] S. Xu, X. Li, Y.T. Hsu, B. Swingle and S. Das Sarma, *Butterfly effect in interacting Aubry-Andre model: thermalization, slow scrambling, and many-body localization*, *arXiv e-prints* (Feb, 2019) arXiv:1902.07199 [[arXiv:1902.07199](#)].
- [7] I.V. Protopopov, R.K. Panda, T. Parolini, A. Scardicchio, E. Demler and D.A. Abanin, *Non-Abelian symmetries and disorder: a broad non-ergodic regime and anomalous thermalization*, *arXiv e-prints* (Feb, 2019) arXiv:1902.09236 [[arXiv:1902.09236](#)].
- [8] X. Chen, T. Zhou, D.A. Huse and E. Fradkin, *Out-of-time-order correlations in many-body localized and thermal phases*, *Annalen der Physik* **529** (Jul, 2017) 1600332 [[arXiv:1610.00220](#)].
- [9] V. Khemani, A. Vishwanath and D.A. Huse, *Operator Spreading and the Emergence of Dissipative Hydrodynamics under Unitary Evolution with Conservation Laws*, *Physical Review X* **8** (Jul, 2018) 031057 [[arXiv:1710.09835](#)].
- [10] Y. Huang, Y.L. Zhang and X. Chen, *Out-of-time-ordered correlators in many-body localized systems*, *Annalen der Physik* **529** (Jul, 2017) 1600318 [[arXiv:1608.01091](#)].
- [11] R. Fan, P. Zhang, H. Shen and H. Zhai, *Out-of-Time-Order Correlation for Many-Body Localization*, *arXiv e-prints* (Aug, 2016) arXiv:1608.01914 [[arXiv:1608.01914](#)].
- [12] Y. Chen and G. Vidal, *Entanglement contour*, *Journal of Statistical Mechanics: Theory and Experiment* **2014** (Oct, 2014) 10011 [[arXiv:1406.1471](#)].
- [13] J. Kudler-Flam, H. Shapourian and S. Ryu, *The negativity contour: a quasi-local measure of entanglement for mixed states*, *arXiv e-prints* (Aug, 2019) arXiv:1908.07540 [[arXiv:1908.07540](#)].
- [14] Q. Wen, *Fine structure in holographic entanglement and entanglement contour*, *arXiv e-prints* (Mar, 2018) arXiv:1803.05552 [[arXiv:1803.05552](#)].
- [15] J. Kudler-Flam, I. MacCormack and S. Ryu, *Holographic entanglement contour, bit threads, and the entanglement tsunami*, *Journal of Physics A: Mathematical and Theoretical* **52** (Jul, 2019) 325401 [[arXiv:1902.04654](#)].

- [16] Q. Wen, *Entanglement contour from subset entanglement entropies*, *arXiv e-prints* (Feb, 2019) arXiv:1902.06905 [[arXiv:1902.06905](#)].
- [17] Q. Wen, *Formulas for Partial Entanglement Entropy*, *arXiv e-prints* (Oct, 2019) arXiv:1910.10978 [[arXiv:1910.10978](#)].
- [18] A.I. Larkin and Y.N. Ovchinnikov, *Quasiclassical Method in the Theory of Superconductivity*, *Soviet Journal of Experimental and Theoretical Physics* **28** (Jun, 1969) 1200.
- [19] S.H. Shenker and D. Stanford, *Black holes and the butterfly effect*, *Journal of High Energy Physics* **2014** (Mar, 2014) 67 [[arXiv:1306.0622](#)].
- [20] D.A. Roberts and D. Stanford, *Diagnosing Chaos Using Four-Point Functions in Two-Dimensional Conformal Field Theory*, *Phys. Rev. Lett.* **115** (Sep, 2015) 131603 [[arXiv:1412.5123](#)].
- [21] J. Maldacena, S.H. Shenker and D. Stanford, *A bound on chaos*, *Journal of High Energy Physics* **2016** (Aug, 2016) 106 [[arXiv:1503.01409](#)].
- [22] M.D. Choi, *Completely positive linear maps on complex matrices*, *Linear Algebra and its Applications* **10** (1975) 285 .
- [23] A. Jamiolkowski, *Linear transformations which preserve trace and positive semidefiniteness of operators*, *Reports on Mathematical Physics* **3** (1972) 275 .
- [24] P. Zanardi, *Entanglement of quantum evolutions*, *Phys. Rev. A* **63** (Apr, 2001) 040304 [[quant-ph/0010074](#)].
- [25] T.c.v. Prosen and I. Pi žorn, *Operator space entanglement entropy in a transverse ising chain*, *Phys. Rev. A* **76** (Sep, 2007) 032316.
- [26] P. Hosur, X.L. Qi, D.A. Roberts and B. Yoshida, *Chaos in quantum channels*, *Journal of High Energy Physics* **2016** (Feb, 2016) 4 [[arXiv:1511.04021](#)].
- [27] J. Kudler-Flam, M. Nozaki, S. Ryu and M. Tian Tan, *Quantum vs. classical information: operator negativity as a probe of scrambling*, *arXiv e-prints* (Jun, 2019) arXiv:1906.07639 [[arXiv:1906.07639](#)].
- [28] J. Cardy, *Thermalization and Revivals after a Quantum Quench in Conformal Field Theory*, *Physical Review Letters* **112** (Jun, 2014) 220401 [[arXiv:1403.3040](#)].
- [29] G. Di Giulio, R. Arias and E. Tonni, *Entanglement hamiltonians in 1D free lattice models after a global quantum quench*, *arXiv e-prints* (May, 2019) arXiv:1905.01144 [[arXiv:1905.01144](#)].

- [30] L. Nie, M. Nozaki, S. Ryu and M. Tian Tan, *Signature of quantum chaos in operator entanglement in 2d CFTs*, *arXiv e-prints* (Nov, 2018) arXiv:1812.00013 [[arXiv:1812.00013](#)].
- [31] G. Mandal, R. Sinha and T. Ugajin, *Finite size effect on dynamical entanglement entropy: CFT and holography*, *arXiv e-prints* (Apr, 2016) arXiv:1604.07830 [[arXiv:1604.07830](#)].
- [32] F. Iglói, Z. Szatmári and Y.C. Lin, *Entanglement entropy dynamics of disordered quantum spin chains*, *Phys. Rev. B* **85** (Mar, 2012) 094417 [[arXiv:1201.3695](#)].
- [33] M. Serbyn, Z. Papić and D.A. Abanin, *Universal Slow Growth of Entanglement in Interacting Strongly Disordered Systems*, *Phys. Rev. Lett.* **110** (Jun, 2013) 260601 [[arXiv:1304.4605](#)].
- [34] J.H. Bardarson, F. Pollmann and J.E. Moore, *Unbounded Growth of Entanglement in Models of Many-Body Localization*, *Phys. Rev. Lett.* **109** (Jul, 2012) 017202 [[arXiv:1202.5532](#)].
- [35] C.J. Lin and O.I. Motrunich, *Out-of-time-ordered correlators in a quantum Ising chain*, *Phys. Rev. B* **97** (Apr, 2018) 144304 [[arXiv:1801.01636](#)].
- [36] S. Byju, K. Lochan and S. Shankaranarayanan, *Generalized thermalization in quenched free Fermionic models*, *arXiv e-prints* (Aug, 2018) arXiv:1808.07742 [[arXiv:1808.07742](#)].
- [37] M. McGinley, A. Nunnenkamp and J. Knolle, *Slow growth of out-of-time-order correlators and entanglement in integrable disordered systems*, *arXiv e-prints* (Jul, 2018) arXiv:1807.06039 [[arXiv:1807.06039](#)].
- [38] D.A. Abanin and Z. Papić, *Recent progress in many-body localization*, *Annalen der Physik* **529** (Jul, 2017) 1700169 [[arXiv:1705.09103](#)].
- [39] M. Serbyn, Z. Papić and D.A. Abanin, *Local Conservation Laws and the Structure of the Many-Body Localized States*, *Phys. Rev. Lett.* **111** (Sep, 2013) 127201 [[arXiv:1305.5554](#)].
- [40] J.Z. Imbrie, V. Ros and A. Scardicchio, *Local integrals of motion in many-body localized systems*, *Annalen der Physik* **529** (Jul, 2017) 1600278 [[arXiv:1609.08076](#)].
- [41] J. Smith, A. Lee, P. Richerme, B. Neyenhuis, P.W. Hess, P. Hauke, M. Heyl, D.A. Huse and C. Monroe, *Many-body localization in a quantum simulator with programmable random disorder*, *Nature Physics* **12** (Oct, 2016) 907 [[arXiv:1508.07026](#)].
- [42] R. Islam, R. Ma, P.M. Preiss, M.E. Tai, A. Lukin, M. Rispoli and M. Greiner, *Measuring entanglement entropy through the interference of quantum many-body twins*, *arXiv e-prints* (Sep, 2015) arXiv:1509.01160 [[arXiv:1509.01160](#)].

- [43] A. Lukin, M. Rispoli, R. Schittko, M.E. Tai, A.M. Kaufman, S. Choi, V. Khemani, J. Léonard and M. Greiner, *Probing entanglement in a many-body-localized system*, *Science* **364** (Apr, 2019) 256 [[arXiv:1805.09819](#)].
- [44] M. Žnidarič, T. Prosen and P. Prelovšek, *Many-body localization in the Heisenberg XXZ magnet in a random field*, *Phys. Rev. B* **77** (Feb, 2008) 064426 [[arXiv:0706.2539](#)].
- [45] J. Couch, S. Eccles, P. Nguyen, B. Swingle and S. Xu, *The Speed of Quantum Information Spreading in Chaotic Systems*, *arXiv e-prints* (Aug, 2019) arXiv:1908.06993 [[arXiv:1908.06993](#)].
- [46] E.H. Lieb and D.W. Robinson, *The finite group velocity of quantum spin systems*, *Comm. Math. Phys.* **28** (1972) 251.
- [47] D.A. Roberts and B. Swingle, *Lieb-Robinson and the butterfly effect*, *arXiv e-prints* (Mar, 2016) arXiv:1603.09298 [[arXiv:1603.09298](#)].
- [48] X. Yu, D. Pekker and B.K. Clark, *Finding matrix product state representations of highly excited eigenstates of many-body localized hamiltonians*, *Phys. Rev. Lett.* **118** (Jan, 2017) 017201.
- [49] S.P. Lim and D.N. Sheng, *Many-body localization and transition by density matrix renormalization group and exact diagonalization studies*, *Phys. Rev. B* **94** (Jul, 2016) 045111.
- [50] V. Khemani, F. Pollmann and S.L. Sondhi, *Obtaining highly excited eigenstates of many-body localized hamiltonians by the density matrix renormalization group approach*, *Phys. Rev. Lett.* **116** (Jun, 2016) 247204.
- [51] D.M. Kennes and C. Karrasch, *Entanglement scaling of excited states in large one-dimensional many-body localized systems*, *Phys. Rev. B* **93** (Jun, 2016) 245129.
- [52] M. Serbyn, A.A. Michailidis, D.A. Abanin and Z. Papić, *Power-law entanglement spectrum in many-body localized phases*, *Phys. Rev. Lett.* **117** (Oct, 2016) 160601.
- [53] S. Sahu, S. Xu and B. Swingle, *Scrambling dynamics across a thermalization-localization quantum phase transition*, *arXiv e-prints* (Jul, 2018) arXiv:1807.06086 [[arXiv:1807.06086](#)].
- [54] T. Zhou and D.J. Luitz, *Operator entanglement entropy of the time evolution operator in chaotic systems*, *Phys. Rev. B* **95** (Mar, 2017) 094206 [[arXiv:1612.07327](#)].
- [55] J. Kudler-Flam, L. Nie and S. Ryu, *Conformal field theory and the web of quantum chaos diagnostics*, *arXiv e-prints* (Oct, 2019) arXiv:1910.14575 [[arXiv:1910.14575](#)].

- [56] B. Groisman, S. Popescu and A. Winter, *Quantum, classical, and total amount of correlations in a quantum state*, *Phys. Rev. A* **72** (Sep, 2005) 032317 [[quant-ph/0410091](#)].
- [57] I. Mondragon-Shem, T.L. Hughes, J. Song and E. Prodan, *Topological Criticality in the Chiral-Symmetric AIII Class at Strong Disorder*, *Phys. Rev. Lett.* **113** (Jul, 2014) 046802 [[arXiv:1311.5233](#)].
- [58] G. Refael and J.E. Moore, *Entanglement Entropy of Random Quantum Critical Points in One Dimension*, *Physical Review Letters* **93** (Dec, 2004) 260602 [[cond-mat/0406737](#)].
- [59] G. Refael and J.E. Moore, *Criticality and entanglement in random quantum systems*, *Journal of Physics A Mathematical General* **42** (Dec, 2009) 504010 [[arXiv:0908.1986](#)].
- [60] N. Laflorencie, *Scaling of entanglement entropy in the random singlet phase*, *Physical Review B* **72** (Oct, 2005) 140408 [[cond-mat/0504446](#)].
- [61] M. Fagotti, P. Calabrese and J.E. Moore, *Entanglement spectrum of random-singlet quantum critical points*, *Phys. Rev. B* **83** (Jan, 2011) 045110 [[arXiv:1009.1614](#)].
- [62] D.S. Fisher, *Random antiferromagnetic quantum spin chains*, *Phys. Rev. B* **50** (Aug, 1994) 3799.
- [63] R. Vasseur, A.C. Potter and S.A. Parameswaran, *Quantum criticality of hot random spin chains*, *Phys. Rev. Lett.* **114** (May, 2015) 217201.
- [64] R. Vasseur, A.J. Friedman, S.A. Parameswaran and A.C. Potter, *Particle-hole symmetry, many-body localization, and topological edge modes*, *Phys. Rev. B* **93** (Apr, 2016) 134207.
- [65] G. De Tomasi, D. Trapin, M. Heyl and S. Bera, *Anomalous diffusion in particle-hole symmetric many-body localized systems*, *arXiv e-prints* (Jan, 2020) arXiv:2001.04996 [[arXiv:2001.04996](#)].
- [66] Y. Zhao, F. Andraschko and J. Sirker, *Entanglement entropy of disordered quantum chains following a global quench*, *Phys. Rev. B* **93** (May, 2016) 205146 [[arXiv:1602.04380](#)].
- [67] O. Motrunich, K. Damle and D.A. Huse, *Dynamics and transport in random quantum systems governed by strong-randomness fixed points*, *Phys. Rev. B* **63** (Mar, 2001) 134424.
- [68] P. Calabrese and J. Cardy, *Evolution of entanglement entropy in one-dimensional systems*, *Journal of Statistical Mechanics: Theory and Experiment* **2005** (Apr, 2005) 04010 [[cond-mat/0503393](#)].
- [69] F.J. Dyson, *The dynamics of a disordered linear chain*, *Phys. Rev.* **92** (Dec, 1953) 1331.

- [70] Y.O. Nakagawa, M. Watanabe, H. Fujita and S. Sugiura, *Universality in volume-law entanglement of scrambled pure quantum states*, *Nature Communications* **9** (Apr, 2018) 1635 [[arXiv:1703.02993](#)].
- [71] E. Westerberg, A. Furusaki, M. Sigrist and P.A. Lee, *Low-energy fixed points of random quantum spin chains*, *Phys. Rev. B* **55** (May, 1997) 12578.
- [72] A. Lazarides, A. Das and R. Moessner, *Periodic Thermodynamics of Isolated Quantum Systems*, *Phys. Rev. Lett.* **112** (Apr, 2014) 150401 [[arXiv:1401.0164](#)].
- [73] B. Skinner, J. Ruhman and A. Nahum, *Measurement-Induced Phase Transitions in the Dynamics of Entanglement*, *Physical Review X* **9** (Jul, 2019) 031009 [[arXiv:1808.05953](#)].
- [74] P. Roushan, C. Neill, J. Tangpanitanon, V.M. Bastidas, A. Megrant, R. Barends, Y. Chen, Z. Chen, B. Chiaro, A. Dunsworth, A. Fowler, B. Foxen, M. Giustina, E. Jeffrey, J. Kelly, E. Lucero, J. Mutus, M. Neeley, C. Quintana, D. Sank, A. Vainsencher, J. Wenner, T. White, H. Neven, D.G. Angelakis and J. Martinis, *Spectral signatures of many-body localization with interacting photons*, *arXiv e-prints* (Sep, 2017) arXiv:1709.07108 [[arXiv:1709.07108](#)].
- [75] M. Schreiber, S.S. Hodgman, P. Bordia, H.P. Lüschen, M.H. Fischer, R. Vosk, E. Altman, U. Schneider and I. Bloch, *Observation of many-body localization of interacting fermions in a quasirandom optical lattice*, *Science* **349** (Aug, 2015) 842 [[arXiv:1501.05661](#)].
- [76] T. Brydges, A. Elben, P. Jurcevic, B. Vermersch, C. Maier, B.P. Lanyon, P. Zoller, R. Blatt and C.F. Roos, *Probing Rényi entanglement entropy via randomized measurements*, *Science* **364** (Apr, 2019) 260 [[arXiv:1806.05747](#)].